Ocean inherent optical property estimation from irradiances

Robert A. Leathers and Norman J. McCormick

A method is evaluated for estimating the absorption coefficient a and the backscattering coefficient b_b from measurements of the upward and downward irradiances $E_u(z)$ and $E_d(z)$. With this method, the reflectance ratio $R(z)$ and the downward diffuse attenuation coefficient $K_d(z)$ obtained from $E_u(z)$ and $E_d(z)$ are used to estimate the inherent optical properties R_∞ and K_∞ that are the asymptotic values of $R(z)$ and $K_d(z)$, respectively. For an assumed scattering phase function $\tilde{\beta}$, there are unique correlations between the values of R_∞ and K_∞ and those of a and b_b that can be derived from the radiative transfer equation. Good estimates of a and the Gordon parameter $G = b_b/(a + b_b)$ can be obtained from R_∞ and K_∞ if the true scattering phase function is not greatly different from the assumed function. The method works best in deep, homogeneous waters, but can be applied to some cases of stratified waters. To improve performance in shallow waters where bottom effects are important, the deep- and shallow-measurement reflectance models also are developed.

Key words: Ocean optics, radiative transfer, optical properties, inverse problem.

1. Introduction

Determination of the beam absorption, scattering, and backscattering coefficients a, b, and b_b of natural waters is a primary goal of optical oceanographers. These inherent optical properties[1] (IOP's) affect the ocean surface color, the transfer of heat to the upper ocean, the transmission of photosynthetically available radiation through the water column, and underwater visibility. The value of a is also used in models that predict phytoplankton growth rate and ocean primary production,[2] and *in situ* measurements of a and b_b are necessary to validate remote sensing algorithms designed to monitor IOP's on a global scale.

A common method for determining a is spectrophotometric analysis of discrete water samples.[3] However, this method is time-consuming, has a limited sampling rate, and is subject to errors. Alternatively, a can be determined from *in situ* natural light measurements. Most simply, a can be determined from simultaneous *in situ* monochromatic irradiance and monochromatic scalar irradiance measurements with the Gershun law[4]; however, monochromatic scalar irradiance detectors are not yet readily available. Instead, estimates of a have been made from near-surface irradiance measurements in conjunction with measurements of remote sensing reflectance[5] or estimates of the downward mean cosine of the radiance distribution.[6] However, the former requires additional above-surface measurements and accurate empirical correlations, whereas the latter assumes the downward mean cosine does not change significantly within the surface layer, and both methods are susceptible to wave-induced fluctuations and to ship shadow.

Reflecting-tube instruments make it possible to obtain small-volume *in situ* estimates of a and $c = a + b$,[7] where the beam attenuation coefficient c is the inverse of the mean free path of a photon. Because reflecting-tube instruments are subject to scattering errors, they use a small sampling volume to minimize these errors, and as a result these instruments can break up or fail to collect large optically active aggregates (marine snow), can give high readings that are due to rare events of large particles entering the sensing area, and can have difficulty detecting low constituent concentrations.

In contrast, IOP estimation from natural irradiances can be obtained from large-volume measurements, and therefore small concentrations of constituents, both large and small, can be detected.[8] Another advantage of calculating IOP's from irradiance measurements is that it enables one to obtain

The authors are with the Department of Mechanical Engineering, University of Washington, Box 352600, Seattle, Washington 98195-2600.

Received 10 February 1997; revised manuscript received 11 August 1997.

0003-6935/97/338685-14$10.00/0

Report Documentation Page

Form Approved
OMB No. 0704-0188

1. REPORT DATE	2. REPORT TYPE	3. DATES COVERED
1997		**00-00-1997 to 00-00-1997**

4. TITLE AND SUBTITLE	5a. CONTRACT NUMBER
Ocean inherent optical property estimation from irradiances	5b. GRANT NUMBER
	5c. PROGRAM ELEMENT NUMBER
6. AUTHOR(S)	5d. PROJECT NUMBER
	5e. TASK NUMBER
	5f. WORK UNIT NUMBER
7. PERFORMING ORGANIZATION NAME(S) AND ADDRESS(ES) **University of Washington,Department of Mechanical Engineering,Box 352600,Seattle,WA,98195-2600**	8. PERFORMING ORGANIZATION REPORT NUMBER
9. SPONSORING/MONITORING AGENCY NAME(S) AND ADDRESS(ES)	10. SPONSOR/MONITOR'S ACRONYM(S)
	11. SPONSOR/MONITOR'S REPORT NUMBER(S)

12. DISTRIBUTION/AVAILABILITY STATEMENT
Approved for public release; distribution unlimited

13. SUPPLEMENTARY NOTES

14. ABSTRACT

15. SUBJECT TERMS

16. SECURITY CLASSIFICATION OF:			17. LIMITATION OF ABSTRACT	18. NUMBER OF PAGES	19a. NAME OF RESPONSIBLE PERSON
a. REPORT	b. ABSTRACT	c. THIS PAGE			
unclassified	**unclassified**	**unclassified**		**14**	

the water properties and light field from the same instrument. At the very least, large-volume measurements can be correlated with small-volume measurements to improve the confidence in these estimates. Perhaps the primary advantage of the large-volume methods is that much irradiance data have already been collected and archived that can be reanalyzed with new algorithms for the estimation of a and b_b.

Here we evaluate the estimation of a and b_b from only *in situ* profiles of the upward and downward irradiances $E_u(z)$ and $E_d(z)$ at geometric depths z. We note that Gordon and Boynton[9] demonstrated that good estimates of b are not possible from only irradiance measurements, and for this reason we focus on estimating a and b_b. Our approach is to determine a and b_b through the determination of the reflectance $R(z)$ and the downward diffuse attenuation coefficient $K_d(z)$. The values of $R(z)$ and $K_d(z)$ are used to estimate the IOP's R_∞ and K_∞, which are the values far from the surface of $R(z)$ and $K_d(z)$, respectively. Given a specific scattering phase function $\tilde{\beta}$, there are unique correlations between the values of R_∞ and K_∞ and those of a and b_b that can be derived from the radiative transfer equation.

The relevant equations of radiative transfer are introduced in Section 2. Estimation of R_∞ and K_∞ in deep, homogeneous waters is considered in Section 3, and the method of calculating a and b_b from K_∞ and R_∞ is presented in Sections 4 and 5. The importance of selecting an appropriate scattering phase function is investigated in Section 6, and a simplified algorithm that is independent of the scattering phase function is evaluated in Section 7. In Sections 8 and 9 we consider cases in which the water is optically shallow and inhomogeneous, respectively.

2. Basic Equations

The integrodifferential transfer equation for waters with homogeneous optical properties and no internal sources is

$$\mu \partial L(z, \mu)/\partial z + cL(z, \mu) = b \int_{-1}^{1} \tilde{\beta}(\mu, \mu') L(z, \mu') \mathrm{d}\mu', \tag{1}$$

where $L(z, \mu)$ is the radiance integrated over all azimuthal directions for polar angle $\cos^{-1} \mu$ with respect to the depth z. All quantities in Eq. (1) are implicitly a function of wavelength. The azimuthally integrated scattering phase function $\tilde{\beta}(\mu, \mu')$ is normalized such that its expansion in Legendre polynomials has the form

$$\tilde{\beta}(\mu, \mu') = \frac{1}{2} \sum_{n=0}^{M} (2n + 1) f_n P_n(\mu) P_n(\mu'), \quad f_0 = 1, \tag{2}$$

where f_n are the expansion coefficients, $P_n(\mu)$ are the Legendre polynomials, and M is the degree of scattering anisotropy. The coefficient $f_1 = g$ is the scattering asymmetry factor. The backscattering coefficient,

$$b_b = b \int_{-1}^{0} \tilde{\beta}(\mu, 1) \mathrm{d}\mu, \tag{3}$$

can be calculated from[10]

$$\tilde{b}_b = b_b/b = (1/2)\left[1 - \sum_{n \text{ odd}} (2n + 1) f_n \int_0^1 P_n(\mu) \mathrm{d}\mu\right] \tag{4}$$

once the f_n coefficients are specified. The integral factors in Eq. (4) can be calculated numerically from the recursion relationship $(n + 1) \int_0^1 P_n(\mu) \mathrm{d}\mu = -(n - 2) \int_0^1 P_{n-2}(\mu) \mathrm{d}\mu$, starting with $\int_0^1 P_1(\mu) \mathrm{d}\mu = 0.5$.

The irradiance reflectance $R(z)$ is

$$R(z) = E_u(z)/E_d(z), \tag{5}$$

where $E_u(z)$ and $E_d(z)$ are the upward and downward irradiances:

$$E_u(z) = \int_{-1}^{0} |\mu| L(z, \mu) \mathrm{d}\mu, \tag{6}$$

$$E_d(z) = \int_{0}^{1} \mu L(z, \mu) \mathrm{d}\mu. \tag{7}$$

The downward irradiance diffuse attenuation coefficient K_d is defined by

$$K_d(z) = -\frac{1}{E_d(z)} \frac{\mathrm{d}E_d(z)}{\mathrm{d}z} = -\frac{\mathrm{d} \ln[E_d(z)]}{\mathrm{d}z}. \tag{8}$$

Although the magnitudes of $R(z)$ and $K_d(z)$ near the surface depend on the surface illumination, at large depths in deep homogeneous waters with no internal sources the values of $R(z)$ and $K_d(z)$ approach asymptotic values R_∞ and K_∞, respectively, that are IOP's. To evaluate R_∞ and K_∞, we separate the spatial and angular dependencies in Eq. (1) with the eigenmodes:

$$L(z, \mu) = \phi(\pm \nu_j, \mu) \exp(\mp cz/\nu_j) \tag{9}$$

and use Eq. (2) to find that the discrete eigenfunctions $\phi(\pm \nu_j, \mu)$ satisfy

$$\phi(\pm \nu_j, \mu) = \frac{\omega_0 \nu_j}{2(\nu_j \mp \mu)} \times \sum_{n=0}^{M} (2n + 1) f_n g_n(\pm \nu_j) P_n(\mu), \quad \nu_j > 1, \tag{10}$$

where ω_0 is the single-scattering albedo $\omega_0 = b/c$. The Chandrasekhar polynomials[11] g_n satisfy the recursion formula

$$n g_n(\nu_j) = h_{n-1} \nu_j g_{n-1}(\nu_j) - (n - 1) g_{n-2}(\nu_j), \tag{11}$$

starting with $g_{-1} = 0$ and $g_0 = 1$, where $h_n = (2n + 1)(1 - \omega_0 f_n)$. From the spherical harmonics (P_N) method[12] with N odd and arbitrarily large, the positive eigenvalues ν_j are approximately the roots of

$$g_{N+1}(\nu_j) = 0. \quad (12)$$

With this formalism, the procedure in Appendix A shows that, for deep homogeneous waters, R_∞ and K_∞ satisfy[13]

$$R_\infty = \frac{\int_0^1 \phi(-\nu_1, \mu)\mu d\mu}{\int_0^1 \phi(+\nu_1, \mu)\mu d\mu}, \quad (13)$$

$$K_\infty = c/\nu_1, \quad (14)$$

where ν_1 is the largest positive eigenvalue. Thus R_∞ can be computed directly from only $\tilde{\beta}$ and ω_0, whereas K_∞ can be determined from the values of $\tilde{\beta}$, ω_0, and c. We can avoid the numerical integration in Eq. (13) by utilizing equations for computing the numerator and denominator of Eq. (13) that are given in Ref. 14 [Eq. (22)].

3. Estimation of R_∞ and K_∞ in Deep, Locally Homogeneous Waters

Given the upward and downward irradiance measurements at arbitrary depths z, $R(z)$ is calculated directly from Eq. (5). Values of $K_d(z)$ are calculated from finite differences of $\ln[E_d(z)]$ with respect to z, an approximation that is exact at large depths where $\ln[E_d(z)]$ varies linearly with z. Thus the calculation of $R(z)$ at a specified depth requires the measurement or interpolation of $E_u(z)$ and $E_d(z)$ at that depth, whereas that of $K_d(z)$ requires at least the measurement of $E_d(z)$ at two depths.

In optically deep, source-free, and homogeneous waters, the vertical profiles of $R(z)$ and $K_d(z)$ approach the asymptotic values R_∞ and K_∞ that we seek. The simplest approach to estimate R_∞ and K_∞ is to calculate $R(z)$ and $K_d(z)$, preferably at large depths, and take $R_\infty = R(z)$ and $K_\infty = K_d(z)$. We refer to this as the asymptotic method (AM) since the approximation is exact in the asymptotic regime. The accuracy of this method depends on the degree to which the light field differs from the asymptotic field and on the noise in the irradiance measurements.

If measurement noise were negligible, the AM would be essentially exact at sufficiently large depths. For illustration, consider the case in which the incident radiation is composed of 70% direct beam and 30% diffuse skylight and the cosine of the angle of the direct beam is $\mu_0 = 0.866$. The corresponding upper-boundary condition just above the sea surface can be modeled as a superposition of direct sunlight, defined with a Dirac delta function, and diffuse skylight:

$$L(0^-, \mu) = 0.7\delta(\mu - 0.866) + 0.3, \quad 0 \le \mu \le 1. \quad (15)$$

Let $\omega_0 = 0.7$ and let the scattering be characterized by the Henyey–Greenstein scattering phase function[15] $\tilde{\beta}_{HG}$, for which $f_n = g^n$, with the scattering asymmetry factor $g = 0.85$. We take the 200th-order scattering anisotropy ($M = 200$) and an index of refraction of 1.34. From Eqs. (13) and (14), we calculate $R_\infty = 0.04119$ and $K_\infty/c = 0.4707$. The value of K_∞ is normalized by c so that the result depends only on ω_0 and the f_n values. Let the vertical distance be measured in optical depths $\tau = cz$ and take the water to be very deep (50 optical depths) with a purely absorbing bottom. As shown in Fig. 1, the profiles of $R(\tau)$ and $K_d(\tau)/c$ converge to their asymptotic values. The profiles shown in Fig. 1 were computed with the discrete ordinates radiative transfer code DISORTB,[16,17] which takes into account the index of refraction mismatch at the surface. The magnitudes of $R(\tau)$ and $K_d(\tau)/c$ below $\tau = 2$ each vary over a range of approximately 6% and below $\tau = 4$ vary by less than 3%. This small range of $R(\tau)$ and $K_d(\tau)$ values away from the surface is typical and aids in the estimation of K_∞/c and R_∞.

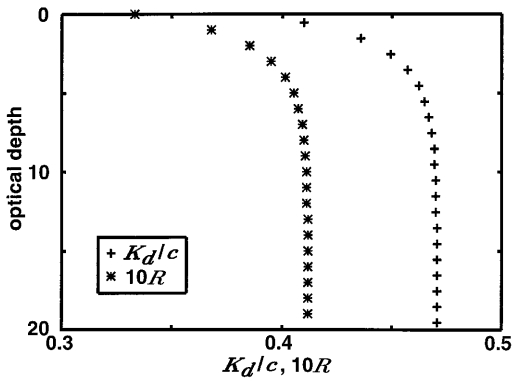

Fig. 1. Diffuse attenuation coefficient and irradiance reflectance profiles from simulated irradiance data ($\omega_0 = 0.7, g = 0.85$). The values of R are multiplied by 10.

Table 1 shows the error in values of R_∞ and K_∞ predicted by the AM from the simulated data shown in Fig. 1. Irradiance values at 1 optical depth vertical spacing were used to calculate $K_d(\tau)$. The errors in the predictions decrease monotonically with depth. However, note that predictions from measurements below 4 optical depths are accurate to within a few percent. This indicates that even

Table 1. Predictions of K_∞ and R_∞ from the Simulated $K_d(\tau)$ and $R(\tau)$ Profiles of Fig. 1 versus the Depth of the Deepest Irradiance Measurement

	Error (%)			
	AM[a]		EM[a]	
τ	R_∞	K_∞/c	R_∞	K_∞/c
3	4.0	4.5	0.78	1.3
4	2.5	2.8	0.32	0.48
5	1.6	1.8	0.12	0.19
7	0.68	0.75	0.012	0.018

[a]Estimates are made from the deepest values of $R(\tau)$ and $K_d(\tau)$ (AM) and from extrapolation with an exponential model (EM) for $K_d(\tau)$ and $R(\tau)$.

though the AM is only theoretically exact at large depths, it can produce good estimates from relatively shallow measurements.

In practice, irradiance measurements contain noise. Consider random noise r in the irradiance measurements that is proportional to the irradiance magnitude. The measured reflectance $R^m(z)$ is

$$R^m(z) = \left(1 + \frac{r_u - r_d}{1 + r_d}\right) R(z), \tag{16}$$

where $R(z)$ is the true reflectance and r_u and r_d are the uncorrelated random noise in the upward and downward irradiance measurements, respectively, after any smoothing or averaging of the data. The measured downward diffuse attenuation coefficient is

$$K_d{}^m(z) = K_d(z) - \mathrm{d}[\ln(1 + r_d)]/\mathrm{d}z. \tag{17}$$

When the AM is used, the relative error of R_∞ is independent of $R(z)$ whereas that of K_∞ is proportional to $[\Delta z K_d(z)]^{-1}$, where Δz is the vertical spacing between $K_d(z)$ values. For example, if the noise r_d and r_u is normally distributed, then the standard deviations of $(r_u - r_d)/(1 + r_d)$ and $[\ln(1 + r_{d,i+1}) - \ln(1 + r_{d,i})]$ are both approximately $1.4s$ if s is the standard deviation of both r_u and r_d. In such a case, the relative errors in R_∞ and K_∞ at large depths are $1.4s$ and $1.4s/[K_d(z)\Delta z]$, respectively.

In addition to the AM for estimating R_∞ and K_∞, one can use analytical approximations to $R(z)$ (Ref. 18) and $K_d(z)$ (Ref. 19) given by

$$R(z) \approx R_\infty + [R(z_r) - R_\infty]\exp[-\mathcal{P}(z - z_r)], \quad z > z_r, \tag{18}$$

$$K_d(z) \approx K_\infty + [K_d(z_r) - K_\infty]\exp[-\mathcal{P}(z - z_r)], \quad z > z_r, \tag{19}$$

where z_r is some reference depth and the IOP $\mathcal{P}$ can be calculated[20] from $\mathcal{P} = c(\nu_2{}^{-1} - \nu_1{}^{-1})$, where ν_2 is the second largest positive eigenvalue from Eq. (12). Because values of $R(z)$ and $K_d(z)$ are predicted for depths below those of the measurements, we refer to this method as the extrapolation method (EM). At large depths the exponential term in Eqs. (18) and (19) becomes negligible and EM estimates become equal to those from the AM. From values of $R(z)$ at depths z_0, z_1, and z_2, with $z_1 = (z_0 + z_2)/2$, R_∞ can be obtained from Eq. (18) as[20]

$$R_\infty = \frac{R(z_0)R(z_2) - R^2(z_1)}{R(z_0) + R(z_2) - 2R(z_1)}. \tag{20}$$

An analogous equation[19] holds for the determination of K_∞ from Eq. (19).

Estimates of R_∞ and K_∞ from the EM for the noise-free data in Fig. 1 are given in Table 1. Irradiance values at 1 optical depth vertical spacing were used, and the results are presented as a function of the depth of the deepest irradiance value used. All predictions are within 0.8% of the true value and, as expected, improve with increasing depth. This indicates that R_∞ and K_∞ can be estimated from relatively shallow measurements, at least when there is no simulated noise. For example, at $\tau = 3$, R_∞ calculated from the EM is within 0.78% of the true value, whereas R_∞ estimated by the AM is in error by 4%. Similarly, at $\tau = 4$, K_∞ calculated from the EM is within 0.48% of the true value, whereas K_∞ estimated by the AM is in error by 2.8%.

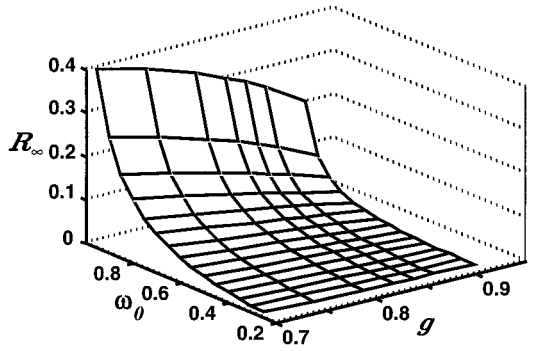

Fig. 2. Interdependence of R_∞, ω_0, and g for $\tilde{\beta}_{\mathrm{HG}}$.

When noise is present, however, estimation of R_∞ and K_∞ from the EM can give improved results over the AM only if the noise in $R(z)$ and $K_d(z)$ is much smaller than the exponential terms in Eqs. (18) and (19) at the depths of the measurements. Thus the extrapolation method may be superior near the surface, but it is inferior to the AM at depths where the true $R(z)$ and $K_d(z)$ vary only slowly with depth. Because our emphasis is on deeper-water applications, the EM is not examined further.

4. Estimation of Fundamental IOP's from R_∞ and K_∞

The parameters a, b, and b_b are fundamental IOP's. In addition, Gordon *et al.*[21] showed that $R(\tau)$ at the surface is nearly proportional to the ratio $b_b/(a + b_b)$, and many remote sensing algorithms are designed to measure either b_b/a or $b_b/(a + b_b)$. We choose to define the ratio $G = b_b/(a + b_b)$ as the (dimensionless) Gordon parameter in view of his many contributions to the field of ocean optics and his observation of the importance of G in remote sensing applications.

If the scattering phase function $\tilde{\beta}$ is assumed, then a and b_b can be determined from measurements of R_∞ and K_∞. The first step in the solution of this inverse problem is to calculate ω_0 from R_∞ and $\tilde{\beta}$, or from R_∞ and g if the phase function $\tilde{\beta}_{\mathrm{HG}}$ is assumed. For example, Fig. 2 shows the interdependence of R_∞, ω_0, and g for the phase function $\tilde{\beta}_{\mathrm{HG}}$. Although in a typical forward calculation R_∞ depends on ω_0 and g, in this inverse problem R_∞ is a measured quantity. The value of $\omega_0(R_\infty, g)$ can be found from an iterative solution of Eq. (13) with the help of Eqs. (10)–(12), and in the process the value of ν_1 is calculated from Eq. (12). Next, c is calculated from ν_1 and the measured value of K_∞ from Eq. (14), a and b are calculated from ω_0 and c, and b_b is computed from Eq. (4) with use of $f_n = g^n$ with the assumed g. Finally, ratios such as b_b/a and $b_b/(a + b_b)$ can be formed from a and b_b.

Table 2. Percent Errors in the Estimates of IOP's for Selected Values of Percent Errors in R_∞ and K_∞

Error (%)					
R_∞	K_∞	a	b and b_b	b_b/a	G
5	0	−1.04	3.32	4.41	4.06
−5	0	1.08	−3.38	−4.41	−4.08
5	5	3.91	8.49	4.41	4.06
−5	5	6.14	1.45	−4.41	−4.08
5	−5	−5.99	−1.84	4.41	4.06
−5	−5	−3.97	−8.21	−4.41	−4.08
0	5	5.00	5.00	0	0

Table 2 gives example calculations of the errors in the estimated values of a, b_b, b_b/a, and G obtained from various values of R_∞ and K_∞ when the true IOP's are $\omega_0 = 0.7$ and $g = 0.85$. These computations were performed with $a = 0.15$ and $b = 0.35$ and the correct phase function and by an iterative search for the optimal value of ω_0. We achieved the search by minimizing the error in the calculated value of R_∞ with respect to ω_0 using Brent's method,[22] which is a combination of an inverse parabolic interpolation and a golden-section search. It can be seen that the errors in the calculations of the fundamental IOP's are of the same order of magnitude as the errors in R_∞ and K_∞. Estimates of a are best when the errors in R_∞ and K_∞ have the same sign, whereas estimates of b_b are best when the errors in R_∞ and K_∞ have the opposite sign. As can be seen from Table 2, b_b/a and G do not depend on K_∞ since $b_b/a = \tilde{b}_b\omega_0(1 - \omega_0)^{-1}$ and $G = [1 + (1 - \omega_0)/(\omega_0\tilde{b}_b)]^{-1}$ and ω_0 is independent of K_∞.

In practice, $\tilde{\beta}$ is not well known, and therefore estimates of ω_0 and c (and of a and b_b) will contain errors that are due both to measurement errors in R_∞ and K_∞ and to the error in the assumed $\tilde{\beta}$. Table 3 shows the percent errors in estimates of a and b_b calculated with the same iterative solution code as for Table 2 but with unknown g and for R_∞ and K_∞ that were computed for the indicated values of ω_0 and g. For the assumed $g = 0.85$, the values of a and b_b are underestimated when the true $g < 0.85$, are exact when $g = 0.85$, and are overestimated when $g > 0.85$. For this large range of g, the worst estimate of a was

Table 3. Percent Errors in the Estimates of a and b_b for Waters with Given Values of g and ω_0[a]

	Error (%)					
	$\omega_0 = 0.5$		$\omega_0 = 0.7$		$\omega_0 = 0.9$	
g	a	b_b	a	b_b	a	b_b
0.75	−1.6	−8.9	−1.2	−9.6	−0.52	−9.8
0.80	−0.83	−4.4	−0.65	−4.9	−0.30	−5.1
0.90	0.86	3.7	0.78	4.6	0.45	5.3
0.95	1.6	6.1	1.7	7.9	1.2	10

[a]The estimates were obtained assuming $g = 0.85$ and using the R_∞ and K_∞ values for the indicated g and ω_0.

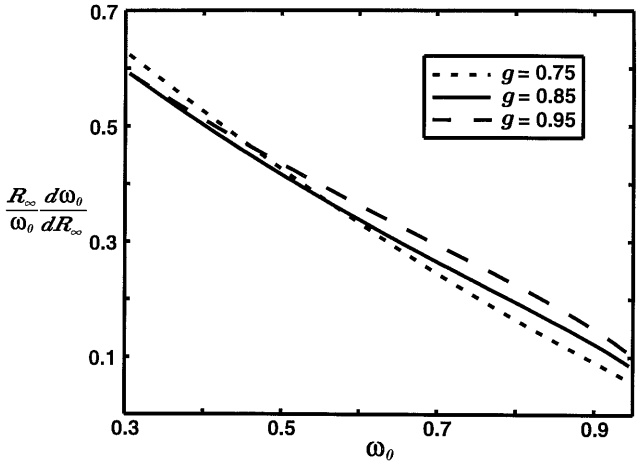

Fig. 3. Normalized sensitivity coefficient of ω_0 with respect to R_∞ for g of $\tilde{\beta}_{HG}$.

in error by only 1.5%, whereas those for b_b were generally within 10%.

To assess more thoroughly the accuracy of predicting fundamental IOP's from R_∞ and K_∞, in Section 5 we examine the sensitivity coefficients that quantify the extent to which errors in R_∞, K_∞, and g affect the estimates of the fundamental IOP's.

5. Sensitivity Coefficients

Normalized sensitivity coefficients express the ratio of the relative error in an output (e.g., a) to a small relative error in an input (e.g., R_∞). In the development of equations for sensitivity coefficients in this section, it is assumed that the phase function can be expressed as a function of a single parameter, such as the scattering asymmetry factor g of the Henyey–Greenstein phase function that is used for the numerical calculations.

A. Sensitivity Coefficients for ω_0 and c

From the iterative search method discussed in Section 4, one can numerically solve for $(R_\infty/\omega_0)(\partial\omega_0/\partial R_\infty)$ and $(g/\omega_0)(\partial\omega_0/\partial g)$. These normalized sensitivity coefficients quantitatively express the sensitivity of the estimates of ω_0 to errors in the measurement of R_∞ and in the guess for g, respectively. Furthermore, these coefficients are required to calculate the sensitivity coefficients for the other fundamental IOP's. As shown in Appendix B, these sensitivity coefficients can also be expressed in terms of sensitivity coefficients for the forward problem. Because the forward problem is much easier to compute than the inverse problem, $(R_\infty/\omega_0)(\partial\omega_0/\partial R_\infty)$ and $(g/\omega_0)(\partial\omega_0/\partial g)$ were computed with Eqs. (B1) and (B2).

In Fig. 3 $(R_\infty/\omega_0)(\partial\omega_0/\partial R_\infty)$ is shown as a function of ω_0. For $0.75 < g < 0.95$, this normalized sensitivity coefficient varies roughly linearly from approximately 0.7 for $\omega_0 = 0.2$ to 0.05 for $\omega_0 = 0.99$. This indicates that estimates of ω_0 from R_∞ are moderately insensitive to small errors in R_∞ and are least sensitive where the absorption relative to the beam attenuation is lowest. The sensitivity coefficient itself is

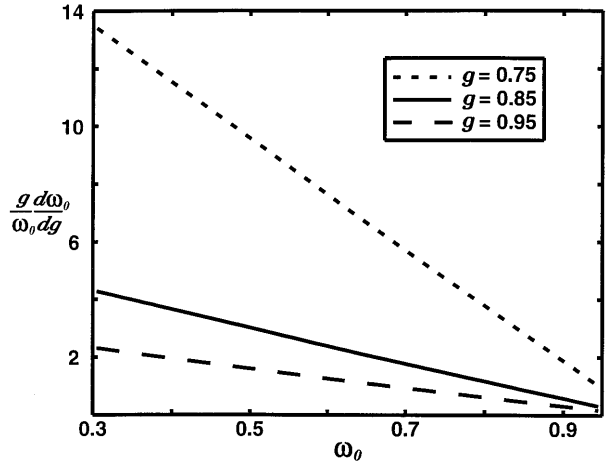

Fig. 4. Normalized sensitivity coefficient of ω_0 with respect to g of $\tilde{\beta}_{HG}$.

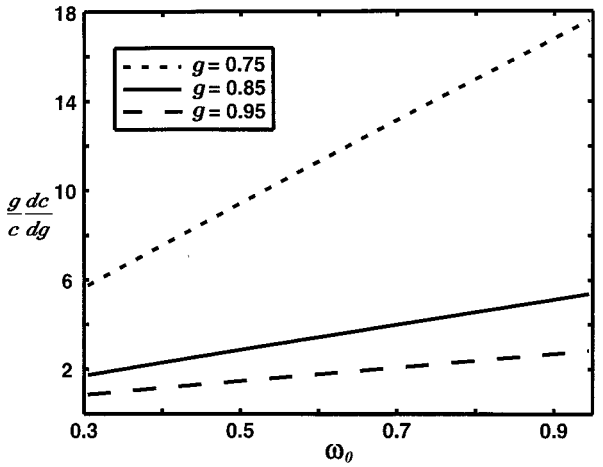

Fig. 6. Normalized sensitivity coefficient of c with respect to g of $\tilde{\beta}_{HG}$.

only weakly dependent on g but is highest for small g when $\omega_0 > 0.5$ and for large g when ω_0 is small. Unfortunately, as can be seen in Fig. 4, estimates of ω_0 are much more sensitive to g than to R_∞. The sensitivity of ω_0 to g is highly dependent on both g and ω_0, and it is highest for large g and for small ω_0. Thus the sensitivities of ω_0 to errors in both g and R_∞ are lowest, and therefore estimates of ω_0 will be best, when ω_0 is high. For $\omega_0 = 0.7$ and $g = 0.85$, for example, a 10% uncertainty in g can result in approximately an 18% uncertainty in ω_0, which would be unacceptably large. Much greater errors may result when g is very high ($g > 0.9$), which is typical for the Petzold phase functions.[23] Because we wish to implement this method of estimating IOP's without knowledge of g, the high sensitivity of ω_0 to g places a serious limitation on our ability to estimate ω_0. However, some other IOP's calculated from ω_0, in particular a, are far less sensitive to g.

In the inverse problem, the largest eigenvalue ν_1 is a function of $\omega_0(R_\infty, g)$ and g and therefore can be written alternatively as a function of the independent variables R_∞ and g. The beam attenuation coefficient is found from

$$c = \nu_1(R_\infty, g)K_\infty, \tag{21}$$

but henceforth the dependence of ν_1 and ω_0 on R_∞ and g will not be denoted explicitly. Note that K_∞ is a measured and therefore independent quantity. One can evaluate the normalized sensitivity coefficients for c from Eq. (21):

$$\frac{K_\infty}{c}\frac{\partial c}{\partial K_\infty} = \frac{K_\infty}{c}\nu_1 = 1, \tag{22}$$

$$\frac{R_\infty}{c}\frac{\partial c}{\partial R_\infty} = \frac{R_\infty}{c}K_\infty\frac{\partial \nu_1}{\partial R_\infty} = \frac{R_\infty}{\nu_1}\frac{\partial \nu_1}{\partial R_\infty}, \tag{23}$$

$$\frac{g}{c}\frac{\partial c}{g} = \frac{gK_\infty}{c}\frac{\partial \nu_1}{\partial g} = \frac{g}{\nu_1}\frac{\partial \nu_1}{\partial g}. \tag{24}$$

These are expressed in terms of normalized sensitivity coefficients $(R_\infty/\nu_1)(\partial\nu_1/\partial R_\infty)$ and $(g/\nu_1)(\partial\nu_1/\partial g)$, which must be computed either from an iterative solution method or, more easily, from Eqs. (B3) and (B4). The magnitude of $(R_\infty/c)(\partial c/\partial R_\infty)$, shown in Fig. 5, is typically less than unity, except for high ω_0 and low g, and is especially low when ω_0 is low. However, the sensitivity of c to g, shown in Fig. 6, is similar in magnitude to that of ω_0 to g, except that it is lowest for low values of ω_0 and highest for high values of ω_0.

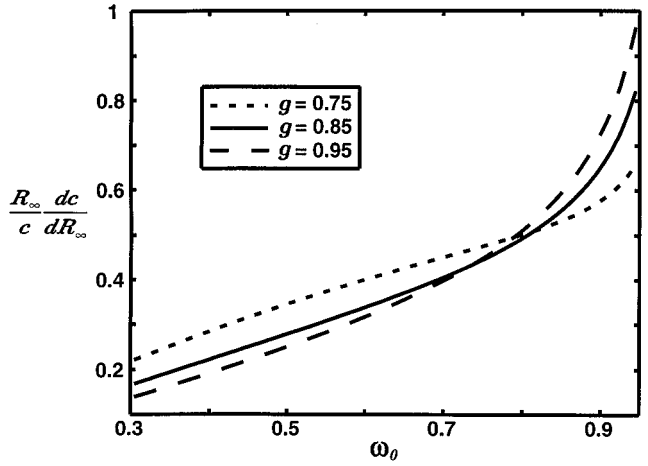

Fig. 5. Normalized sensitivity coefficient of c with respect to R_∞ for g of $\tilde{\beta}_{HG}$.

B. Sensitivity Coefficients for a, b_b, b_b/a, and G

Because

$$a = c(1 - \omega_0), \quad \partial a/\partial\omega_0 = -c, \quad \partial a/\partial c = (1 - \omega_0), \tag{25}$$

$$b = c\omega_0, \qquad \partial b/\partial\omega_0 = c, \qquad \partial b/\partial c = \omega_0, \tag{26}$$

the normalized sensitivity coefficients for a can be determined directly from those for ω_0 (Figs. 3 and 4) and c [Eqs. (22)–(24)]:

$$\frac{K_\infty}{a}\frac{\partial a}{\partial K_\infty} = \frac{K_\infty}{a}\frac{\partial a}{\partial c}\frac{\partial c}{\partial K_\infty} = \frac{K_\infty}{a}(1-\omega_0)\nu_1 = 1, \tag{27}$$

$$\frac{R_\infty}{a}\frac{\partial a}{\partial R_\infty} = \frac{R_\infty}{a}\left[\frac{\partial a}{\partial c}\frac{c}{R_\infty}\left(\frac{R_\infty}{c}\frac{\partial c}{\partial R_\infty}\right) + \frac{\partial a}{\partial \omega_0}\frac{\omega_0}{R_\infty}\left(\frac{R_\infty}{\omega_0}\frac{\partial \omega_0}{\partial R_\infty}\right)\right]$$
$$= \left(\frac{R_\infty}{c}\frac{\partial c}{\partial R_\infty}\right) - \left(\frac{\omega_0}{1-\omega_0}\right)\left(\frac{R_\infty}{\omega_0}\frac{\partial \omega_0}{\partial R_\infty}\right), \tag{28}$$

$$\frac{g}{a}\frac{\partial a}{\partial g} = \frac{g}{a}\left[\frac{\partial a}{\partial c}\frac{c}{g}\left(\frac{g}{c}\frac{\partial c}{\partial g}\right) + \frac{\partial a}{\partial \omega_0}\frac{\omega_0}{g}\left(\frac{g}{\omega_0}\frac{\partial \omega_0}{\partial g}\right)\right]$$
$$= \left(\frac{g}{c}\frac{\partial c}{\partial g}\right) - \left(\frac{\omega_0}{1-\omega_0}\right)\left(\frac{g}{\omega_0}\frac{\partial \omega_0}{\partial g}\right). \tag{29}$$

Similarly, the normalized sensitivity coefficients for b are

$$\frac{K_\infty}{b}\frac{\partial b}{\partial K_\infty} = \frac{K_\infty}{b}\omega_0\nu_1 = 1, \tag{30}$$

$$\frac{R_\infty}{b}\frac{\partial b}{\partial R_\infty} = \frac{R_\infty}{b}\left[\frac{\partial b}{\partial c}\frac{c}{R_\infty}\left(\frac{R_\infty}{c}\frac{\partial c}{\partial R_\infty}\right) + \frac{\partial b}{\partial \omega_0}\frac{\omega_0}{R_\infty}\left(\frac{R_\infty}{\omega_0}\frac{\partial \omega_0}{\partial R_\infty}\right)\right]$$
$$= \left(\frac{R_\infty}{c}\frac{\partial c}{\partial R_\infty}\right) + \left(\frac{R_\infty}{\omega_0}\frac{\partial \omega_0}{\partial R_\infty}\right), \tag{31}$$

$$\frac{g}{b}\frac{\partial b}{\partial g} = \frac{g}{b}\left[\frac{\partial b}{\partial c}\frac{c}{g}\left(\frac{g}{c}\frac{\partial c}{\partial g}\right) + \frac{\partial b}{\partial \omega_0}\frac{\omega_0}{g}\left(\frac{g}{\omega_0}\frac{\partial \omega_0}{\partial g}\right)\right]$$
$$= \left(\frac{g}{c}\frac{\partial c}{\partial g}\right) + \left(\frac{g}{\omega_0}\frac{\partial \omega_0}{\partial g}\right). \tag{32}$$

Thus, all else being equal, the percent error in a and b that is due to an error in K_∞ is equal to the percent error in K_∞. The normalized sensitivity coefficients for b to R_∞ and g are equal to the sum of those for c and ω_0 to R_∞ and g, respectively, whereas the expressions for the normalized sensitivity coefficients for a to R_∞ and g are similar to those for b except that for a the coefficients involving ω_0 are scaled by $-\omega_0/(1-\omega_0) = -b/a$. Note that because $\partial c/\partial R_\infty$ and $\partial \omega_0/\partial R_\infty$ have the same sign, the sensitivity coefficients for a are less than those for b, which is consistent with the observation in Section 4.

The coefficient $(g/a)(\partial a/\partial g)$ is shown in Fig. 7. The absolute value of the magnitude of the coefficient is very low (<0.16) for $\omega_0 < 0.99$. It is highly dependent on ω_0, with the largest magnitude corresponding to moderate values of ω_0. The coefficient $(R_\infty/a)(\partial a/\partial R_\infty)$ is shown in Fig. 8. This coefficient also is relatively small, with typical values ranging from -0.1 to -0.6 for $\omega_0 < 0.9$. Therefore, even though a is calculated from ω_0 and c, each of which are poorly estimated from R_∞ and K_∞, a can be calculated quite well. As expected, the sensitivity of b to g as calculated from Eq. (32) is very large, especially for large

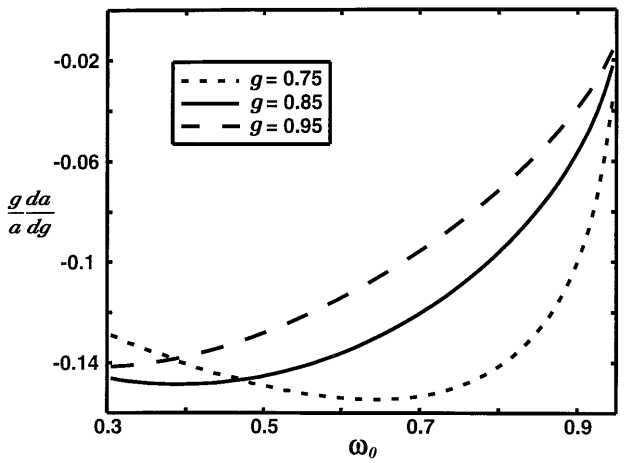

Fig. 7. Normalized sensitivity coefficient of a with respect to g of $\tilde{\beta}_{HG}$.

values of g, and therefore reasonable estimates of b when $\tilde{\beta}$ is not known are not possible.

The normalized sensitivity coefficient of b_b to g is the sum of those of b to g and $\tilde{b}_b$ to g:

$$\frac{g}{b_b}\frac{\partial b_b}{\partial g} = \frac{g}{b}\frac{\partial b}{\partial g} + \frac{g}{\tilde{b}_b}\frac{\partial \tilde{b}_b}{\partial g}. \tag{33}$$

This introduces a fifth sensitivity coefficient $(g/\tilde{b}_b)(\partial \tilde{b}_b/\partial g)$ that must be computed numerically. A plot of $(g\partial b_b)/(b_b\partial g)$ is shown in Fig. 9. The terms $(g/b)(\partial b/\partial g)$ and $(g/\tilde{b}_b)(\partial \tilde{b}_b/\partial g)$ tend to cancel out because the signs are different, so estimates of b_b are moderately insensitive to g [$0.4 < |(g\partial b_b)/(b_b\partial g)| < 0.9$], indicating that estimates of b_b will be reasonable even if g is not well known. Because $b_b = \tilde{b}_b b$, the normalized sensitivity coefficient of b_b to K_∞ is unity, whereas that of b_b to R_∞ is identical to that for b given in Eq. (31) and is shown in Fig. 10.

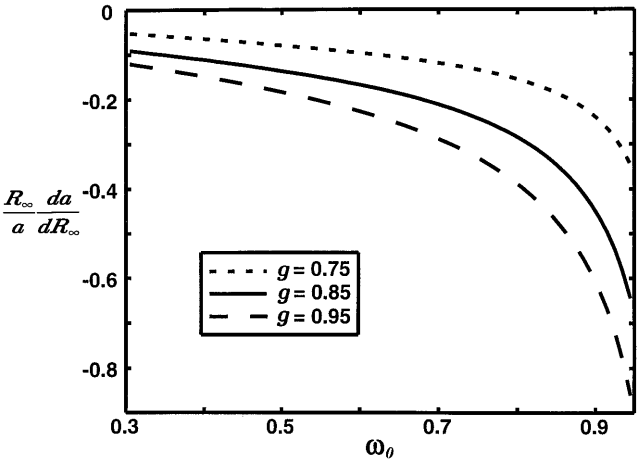

Fig. 8. Normalized sensitivity coefficient of a with respect to R_∞ for g of $\tilde{\beta}_{HG}$.

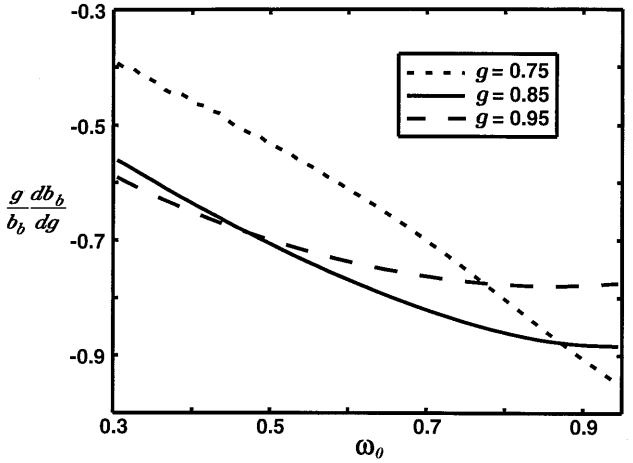

Fig. 9. Normalized sensitivity coefficient of b_b with respect to g of $\tilde{\beta}_{\mathrm{HG}}$.

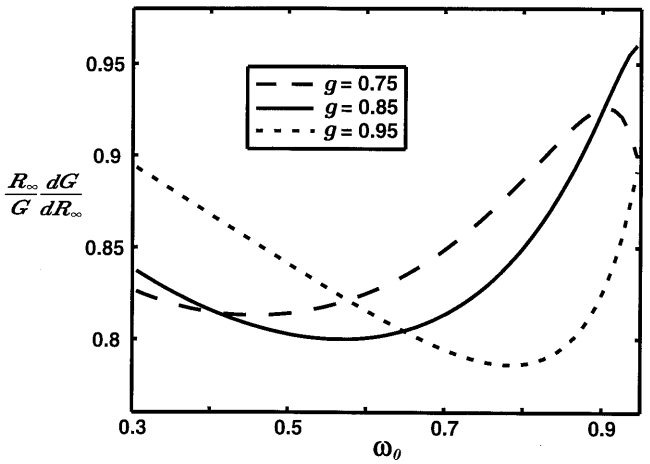

Fig. 11. Normalized sensitivity coefficient of G with respect to R_∞ for g of $\tilde{\beta}_{\mathrm{HG}}$.

Recall that both b_b/a and G are independent of K_∞. The normalized sensitivity coefficient of b_b/a to g is

$$\frac{g}{(b_b/a)}\frac{\partial(b_b/a)}{\partial g} = \frac{g}{b_b}\frac{\partial b_b}{\partial g} - \frac{g}{a}\frac{\partial a}{\partial g} = \frac{g}{\tilde{b}_b}\frac{\partial \tilde{b}_b}{\partial g} + \frac{1}{(1-\omega_0)}\frac{g}{\omega_0}\frac{\partial \omega_0}{\partial g}, \quad (34)$$

and the sensitivity coefficient of G to g is proportional to that of (b_b/a) to g:

$$\frac{g}{G}\frac{\partial G}{\partial g} = \frac{a}{a+b_b}\left[\frac{g}{(b_b/a)}\frac{\partial(b_b/a)}{\partial g}\right]. \quad (35)$$

Because $\partial b_b/\partial g$ and $\partial a/\partial g$ have the same sign and $|(g\partial b_b)/(b_b\partial g)| > |(g\partial a)/(a\partial g)|$, then from Eq. (34) the magnitude of the sensitivity of b_b/a to g is less than that of b_b, and because $a/(a+b_b) < 1$, then from Eq. (35) G is even less sensitive to g than is b_b/a, especially for large ω_0. The normalized sensitivity coefficients of b_b/a and G to R_∞ are in the same form as those to g:

$$\frac{R_\infty}{(b_b/a)}\frac{\partial(b_b/a)}{\partial R_\infty} = \frac{R_\infty}{\tilde{b}_b}\frac{\partial \tilde{b}_b}{\partial R_\infty} + \frac{1}{(1-\omega_0)}\frac{R_\infty}{\omega_0}\frac{\partial \omega_0}{\partial R_\infty}, \quad (36)$$

$$\frac{R_\infty}{G}\frac{\partial G}{\partial R_\infty} = \frac{a}{a+b_b}\left[\frac{R_\infty}{(b_b/a)}\frac{\partial(b_b/a)}{\partial R_\infty}\right]. \quad (37)$$

The sensitivities of G are shown in Figs. 11 and 12.

6. Choice of the Phase Function Model

Equations (29) and (32) hold for any model of the phase function $\tilde{\beta}$ that can be specified by a single parameter g. In Figs. 7 and 9 the one-term Henyey–Greenstein function was used because of its simplicity. Other models could be used, however. For example, phase functions obtained by a combination of the pure seawater phase function and the Petzold particle phase function[24] can also be specified by the

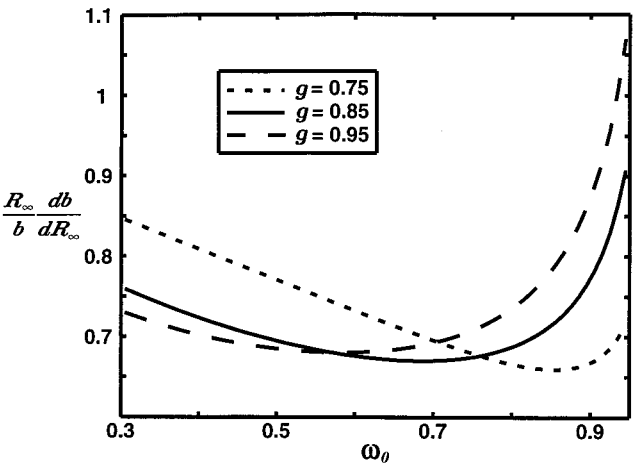

Fig. 10. Normalized sensitivity coefficient of b or b_b with respect to R_∞ for g of $\tilde{\beta}_{\mathrm{HG}}$.

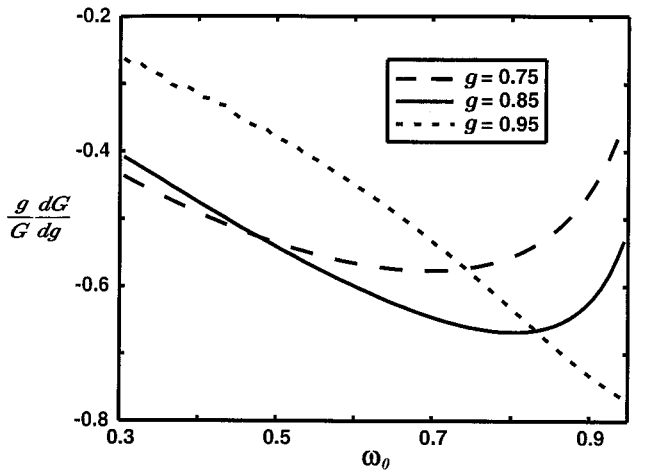

Fig. 12. Normalized sensitivity coefficient of G with respect to g of $\tilde{\beta}_{\mathrm{HG}}$.

value of g or, more commonly, the chlorophyll concentration.

Even if the single parameter defining the phase function model is known, errors may be introduced into the estimates of a and b_b if the shape of the true phase function differs from that predicted by the model. For example, Fig. 13 shows four phase functions that are all characterized by $g = 0.85$ but that have very different shapes in the backscattering directions. These were generated from the two-term Henyey–Greenstein model,[25] which is a linear combination of two one-term Henyey–Greenstein functions:

$$\tilde{\beta}(g_1, g_2, \alpha) = \alpha\tilde{\beta}(g_1) + (1 - \alpha)\tilde{\beta}(g_2), \qquad (38)$$

with parameters g_1, g_2, and α, for $0 \le \alpha \le 1$. Selection of a negative g_2, for example, yields an enhanced backscattering effect. Shown are a, the one-term function ($g_1 = 0.85$, $\alpha = 0$); b, a monotonic function with more backscattering ($g_1 = 0.88$, $g_2 = -0.062$, $\alpha = 0.97$); c, the function whose first three moments match those of the water–Petzold particle mixture model[24] ($g_1 = 0.90$, $g_2 = -0.26$, $\alpha = 0.96$); and d, a case with extremely high backscattering ($g_1 = 0.90, g_2 = -0.64$, $\alpha = 0.97$).

The phase functions in Fig. 13 were used to determine the effect of the amount of backscattering in the assumed phase function on the estimates of the IOP's. Values of R_∞ and K_∞ were first calculated from the forward problem for each of the four phase functions. Then the values of a and b_b were estimated from the R_∞ and K_∞ with the approach in Section 4 assuming either phase function a or c. Table 4 shows the percent errors in the estimated IOP's. Estimates of b_b were several times more sensitive to the assumed $\tilde{\beta}$ than were those of a. Because phase functions a and b are decreasing monotonically in the backscattering direction, estimates of b_b assuming phase function a were in error by as much as 30% when the true $\tilde{\beta}$ exhibits the enhanced backscattering of phase functions c and d. Similarly, assuming phase function c when the true phase function was a or b led to large errors. Conversely, when phase function c was assumed and the true $\tilde{\beta}$ was phase function d, which also exhibits enhanced backscattering, the estimates of a and b_b were in error by only 1.7% and 2.8%, respectively, even though the magnitude of phase function d at 180 deg is several times larger than that of c.

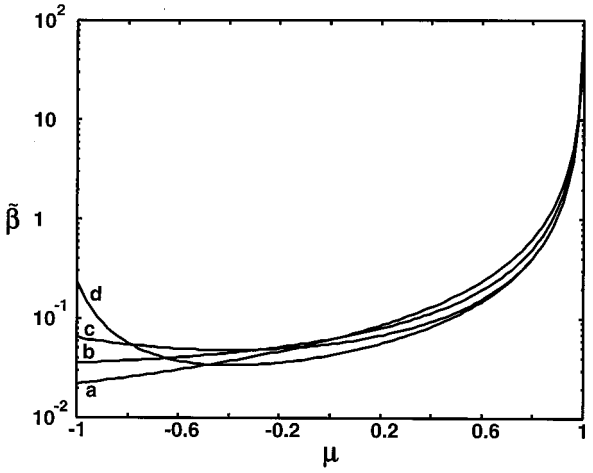

Fig. 13. Two-term Henyey–Greenstein phase function model for $g = 0.85$ and a, $g_1 = 0.85$, $\alpha = 0$; b, $g_1 = 0.88$, $g_2 = -0.062$, $\alpha = 0.97$; c, $g_1 = 0.90$, $g_2 = -0.26$, $\alpha = 0.96$; and d, $g_1 = 0.90$, $g_2 = -0.64$, $\alpha = 0.97$.

Table 4. Percent Errors in the Estimates of IOP's for $\omega_0 = 0.7$ and the Two-Term Henyey–Greenstein Phase Functions Shown in Fig. 13[a]

	Error (%)					
	Assumed $\tilde{\beta}$ Phase Function a			Assumed $\tilde{\beta}$ Phase Function c		
True $\tilde{\beta}$	a	b_b	G	a	b_b	G
a	0.0	0.0	0.0	5.8	−52	−49
b	−2.5	−17	−14	3.1	14	9.5
c	−5.3	−28	−22	0.0	0.0	0.0
d	−6.9	−26	−19	−1.7	2.8	4.0

[a]The assumed $\tilde{\beta}$ is either the one-term phase function a ($\alpha = 0$ and $g_1 = 0.85$) or the two-term function c ($g_1 = 0.90, g_2 = -0.26$, $\alpha = 0.96$). The true phase functions used in the forward calculation of R_∞ and K_∞ are functions a, c, b ($g_1 = 0.88, g_2 = -0.062$, $\alpha = 0.97$), and d ($g_1 = 0.90, g_2 = -0.64$, $\alpha = 0.97$).

These results show that, to obtain good estimates of b_b, it is not sufficient for the assumed phase function to be characterized by an appropriate value of g; the amount of backscattering is also important. In particular, the one-term Henyey–Greenstein function model should not be used in the estimation of b_b in natural waters; the Petzold phase function or a two-term Henyey–Greenstein function similar to c would be better.

7. Phase-Function-Independent Algorithm

Haltrin[26] recognized that a simple model for an approximate phase function $\tilde{\beta}(\mu, \mu') = 2\tilde{b}_b + 2(1 - 2\tilde{b}_b)\delta(\mu - \mu')$ conveys much of the information needed to describe highly forward scattering. For this $\tilde{\beta}$ he derived equations for R_∞ and K_∞/c from a carefully derived two-flux theory:

$$\frac{a}{b_b} = \frac{(1 - \sqrt{R_\infty})^2(1 + 4\sqrt{R_\infty} + R_\infty)}{4R_\infty}, \qquad (39)$$

$$K_\infty/c = (1 - \omega_0)\left\{\frac{1 + G}{1 + 2G - [G(4 + 5G)]^{1/2}}\right\}^{1/2}. \qquad (40)$$

Equation (39) can be used to estimate a/b_b from R_∞, and G can be calculated from $G = (1 + a/b_b)^{-1}$. Then a can be estimated from a rearrangement of Eq. (40):

$$a = K_\infty\left\{\frac{1 + G}{1 + 2G - [G(4 + 5G)]^{1/2}}\right\}^{-1/2}, \qquad (41)$$

which enables one to also obtain b_b. The primary difference between Haltrin's model and that proposed in Section 4 is that in Haltrin's model only two closed-

Table 5. Percent Errors in the Estimates of a and b_b Obtained from Haltrin's Model for $c = 1$ and the One-Term Henyey–Greenstein Phase Function[a]

	Error (%)					
	$\omega_0 = 0.5$		$\omega_0 = 0.7$		$\omega_0 = 0.9$	
g	a	b_b	a	b_b	a	b_b
0.75	2.2	50	2.5	67	1.4	82
0.80	2.8	51	3.2	71	2.0	90
0.85	3.2	50	4.0	73	2.7	98
0.90	3.4	44	4.6	69	3.8	100
0.95	2.8	32	4.5	53	5.2	97

[a]Values of R_∞ and K_∞ were calculated for the given ω_0 and g, and were used to estimate a and b_b from Eqs. (39) and (41).

form analytical equations are needed and no assumption about the phase function is required, whereas in the method proposed in Section 4 an assumed phase function must be incorporated into the iterative solution of Eqs. (10)–(13). Although Eqs. (39) and (41) have the significant advantage in that they are easier to implement in practice, they are less flexible since they do not admit *a priori* information about the phase function.

Table 5 shows the percent errors in estimates of a and b_b obtained from Eqs. (39) and (41) for the one-term Henyey–Greenstein phase function with $0.75 \le g \le 0.95$ and $0.5 \le \omega_0 \le 0.9$. As for Table 3, the values of R_∞ and K_∞ were computed for the given values of ω_0 and g. The calculations were performed for $c = 1$; however, the percent errors in a and b_b were found to be insensitive to the value of c. The errors in the estimates of a range from 1.4% to 5.2%, whereas those in the estimates of b_b range from 32% to 100%. The errors in a are roughly twice those in Table 3 obtained with the approach described in Section 4, whereas the errors in b_b are many times larger. Similar results were obtained with the San Diego Petzold water phase function for a case of 10-mg/m^3 chlorophyll concentration and 685-nm light; for $\omega_0 = 0.5$, 0.7, and 0.9 the percent errors in a were 1.8, 2.6, and 1.9, respectively, and the percent errors in b_b were 44, 61, and 81, respectively.

The large errors in b_b should be expected because of the high sensitivity of b_b to the shape of the backscattering portion of $\tilde{\beta}$ demonstrated in Section 6. The degree to which the $\tilde{\beta}$-dependent approach of Section 4 outperforms Haltrin's approach depends on how well the assumed $\tilde{\beta}$ matches the actual scattering phase function of the water.

8. IOP Estimation in Shallow Waters

In shallow water where the entire water column is in the euphotic zone, profiles $R(z)$ and $K_d(z)$ are affected by the interaction of light with the bottom. Although the effects of the bottom usually do not reach as far into the water column as do surface conditions, bottom effects can cause errors in IOP estimation. If the water is so shallow that significant surface and bottom effects overlap, then $R(z)$ and $K_d(z)$ never reach R_∞ and K_∞, respectively. However, estimates of R_∞ and K_∞ can still be made in water of at least a few optical depths. In this case, $R(z)$ and $K_d(z)$ near the surface tend toward R_∞ and K_∞ with increasing depth and near the bottom deviate away from R_∞ and K_∞. The asymptotic method for estimating R_∞, for example, can be applied by taking $R_\infty = R(z_m)$ at a mid-water-column depth z_m where $R(z)$ is a maximum or minimum or is at an inflection point.

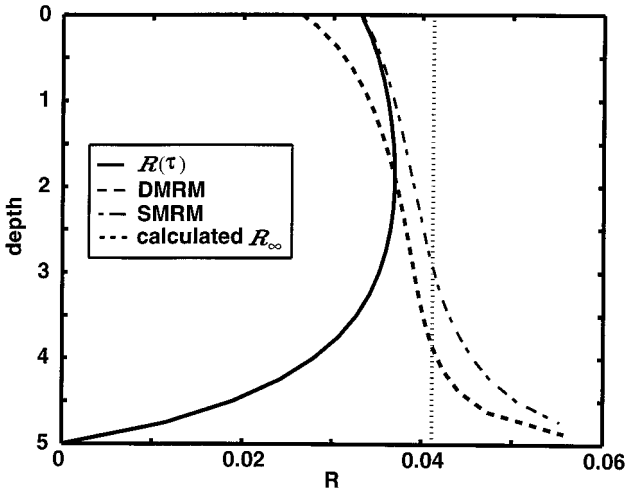

Fig. 14. Estimation of R_∞ in water of 5 optical depths with a purely absorbing bottom ($R_b = 0$). Shown are R_∞ from Eq. (13), the local irradiance ratio $R(\tau)$ that forms the asymptotic model (AM), and the depth-dependent estimates of R_∞ from the deep-measurement reflectance model (DMRM) and the shallow-measurement reflectance model (SMRM).

Figure 14 shows $R(\tau)$ for water of 5 optical depths with a purely absorbing bottom, i.e., the bottom albedo R_b vanishes. This water is characterized by $\omega_0 = 0.70$, $g = 0.85$ and $R_\infty = 0.0412$ based only on the IOP's. From top to bottom, $R(\tau)$ increases from its surface value toward the value of R_∞ and then decreases to the bottom value of $R_b = 0$. The best place to apply the AM in this case is at the maximum $R(\tau)$. Such an estimate will always be shy of the true value, but it is difficult to know by how much, especially from noisy measurements. Figure 15 shows the same water as in Fig. 14, but with a Lambertian reflecting bottom of $R_b = 0.2$. In this case $R(\tau)$ has an inflection point near the depth where $R(\tau) = R_\infty$, although it is barely detectable because of the large bottom effects. Because $R_b \gg R_\infty$, values of $R(\tau)$ deep in the water column are far from R_∞.

To improve our ability to treat shallow waters, two alternative methods for calculating R_∞ from $E_d(z)$ and $E_u(z)$ near the bottom are derived in Appendix C: the deep-measurement reflectance model (DMRM) and the shallow-measurement reflectance model (SMRM). For the DMRM one must make measurements of $E_d(z)$ and $E_u(z)$ at two depths, subtract and add the irradiances at each depth, square the results,

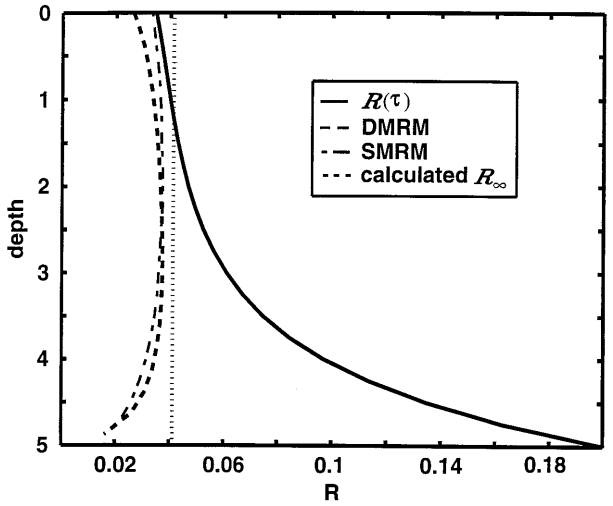

Fig. 15. Estimation of R_∞ as in Fig. 14 for a Lambertian bottom reflectance of $R_b = 0.2$.

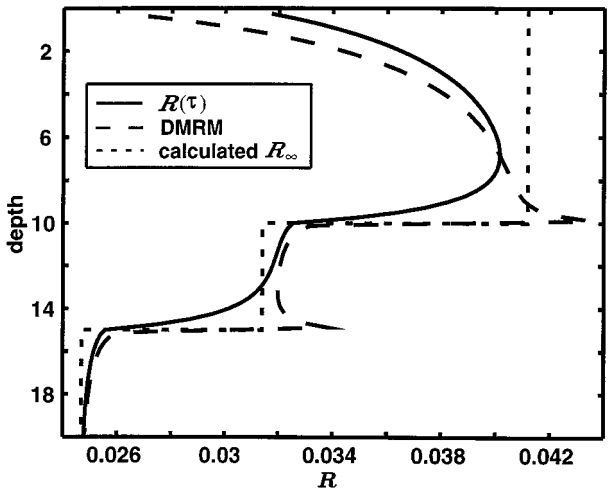

Fig. 16. Estimation of R_∞ in three distinct water layers. From top to bottom, $\omega_0 = 0.7$, 0.65, and 0.60. Shown are R_∞ from Eq. (13), the local irradiance ratio $R(\tau)$, and the estimate of $R_\infty(\tau)$ from the DMRM.

and evaluate the differences at the two depths. The estimated value of R_∞ follows from

$$\left(\frac{1 - R_\infty}{1 + R_\infty}\right)^2 = \frac{[E_d(z) - E_u(z)]^2|_{z_1}^{z_2}}{[E_d(z) + E_u(z)]^2|_{z_1}^{z_2}}. \tag{42}$$

Note that this technique for estimating R_∞ can be especially useful for z near the bottom because it incorporates the growing eigenmode $\tilde{g}_1(\mp\nu_1)\exp(cz/\nu_1)$ (see Appendix C) that is needed to account for the asymptotic contribution of the bottom boundary condition. An advantage of the DMRM is that the bottom albedo R_b need not be known, but a disadvantage is that differences of noisy irradiance measurements potentially can lead to large errors.

For the SMRM one needs to know the bottom albedo R_b and the depth of the water column z_b. From measurements of $R(z)$ at arbitrary geometric depth z, R_∞ can be predicted from

$$R_\infty = \{R(z) - R_b \exp[-2K_d(z)(z_b - z)]\}/ \{1 - \exp[-2K_d(z)(z_b - z)]\}. \tag{43}$$

The values of R_∞ predicted by the AM, where $R_\infty = R(z)$, the DMRM, and the SMRM are shown as a function of depth in Figs. 14 and 15. Estimates of R_∞ from the SMRM require an estimate of K_∞; however, it was found that these estimates are not very sensitive to K_∞, and the approximation $K_\infty = K_d(\tau)$ was used in Figs. 14 and 15. It can be seen that the DMRM method does poorly compared with the AM near the surface but yields much better estimates than the AM below mid-depth. The SMRM method performs better than the DMRM near the surface, but performs worse than the DMRM near the bottom. Both the DMRM and the SMRM give the best estimates of R_∞ at mid-depths, away from both boundaries.

Estimates of $R_\infty(\tau)$ from the DMRM method are more susceptible to noise in the irradiance measurements than are those from the SMRM or AM. However, smoothing of $R_\infty(\tau)$ was found to be effective in reducing this noise in simulated data, making good estimates of R_∞ from the DMRM possible.

Profiles of $K_d(z)$ tend to be less influenced by the bottom depth and albedo than are $R(z)$, especially if the bottom is highly absorbing. Similar to $R(z)$, $K(z)$ tends to be closest to K_∞ at its minimum, maximum, or inflection point. Unfortunately, a shallow-water method such as those for R_∞ could not be developed for K_∞.

9. IOP Estimation in Inhomogeneous Waters

For inhomogeneous waters, R_∞ and K_∞ as computed from Eqs. (13) and (14) now depend on the local IOP's at z, so that $R_\infty(z)$ and $K_\infty(z)$ are a function of depth. If the optical properties vary only gradually with depth, then $R(z) \approx R_\infty(z)$ and $K_d(z) \approx K_\infty(z)$ below the depths where the surface illumination dominates. On the other hand, if the optical properties are highly variable with depth, some type of weighted average of the IOP's can be estimated, but the fine structure cannot be determined accurately.

Figure 16 shows a simulated example of three distinct water layers. For all three layers $g = 0.85$, but $\omega_0 = 0.7$, 0.65, and 0.60, from top to bottom. Shown are R_∞ from Eq. (13), the local irradiance ratio $R(\tau)$, and the estimate of $R_\infty(\tau)$ from the DMRM. The AM for estimating $R_\infty(\tau)$ in the three layers could be applied by one taking the maximum $R(\tau)$ in the upper layer, the inflection point in the middle layer, and the asymptotic value in the deep bottom layer. Because the top two layers in this case are both affected by a distinctly different layer below them, estimates of R_∞ from the DMRM are more accurate than those from the AM just above the interfaces, but are less accurate just below the interfaces. Both methods do a good job of identifying the location of the interfaces.

10. Summary

We have tested numerically an inverse radiative transfer method for estimating two inherent optical

properties from the irradiance ratio $R(z)$ and the downward diffuse attenuation coefficient $K_d(z)$ computed from upward and downward irradiance measurements. The method involves two steps. First, the IOP's R_∞ and K_∞ are estimated from $R(z)$ and $K_d(z)$. Second, IOP's such as a and b_b are calculated from the analytical equations in (13) and (14) for R_∞ and K_∞.

The simplest approach to the first step is to use the AM, where it is assumed $R_\infty = R(z)$ and $K_\infty = K_d(z)$. In deep waters, the exponential method of Eqs. (18) and (19) can yield better results than the AM if only shallow irradiance measurements are available. On the other hand, in shallow waters the DMRM and SMRM reflectance models of Eqs. (42) and (43) yield better estimates for R_∞ than the AM, but we were unable to develop a deep- or shallow-measurement diffuse attenuation coefficient model.

In the second step, a scattering phase function is assumed, and ω_0 is estimated from R_∞ with an iterative search. The values of a and b_b are then calculated from ω_0 and K_∞. This approach was compared with Haltrin's model that relates a and b_b to R_∞ and K_∞ through two closed-form equations (39) and (41). Although Haltrin's model is easier to implement, it is generally less accurate because no *a priori* information about the scattering phase function can be incorporated.

Example numerical calculations and a sensitivity analysis have shown that the absorption coefficient and the Gordon parameter $G = b_b/(a + b_b)$ can be estimated quite well even if the scattering asymmetry factor is unknown. However, it was shown with use of the two-term Henyey–Greenstein phase function that, because b_b is sensitive to the backscattering portion of the phase function, it is important to use a realistic scattering phase model, such as a Petzold phase function, in the inverse solution.

Appendix A: Deep-Water Asymptotic Irradiance Ratio and Diffuse Attenuation Coefficient

The radiance for a source-free (i.e., no fluorescence or Raman scattering effects) homogeneous medium can be expressed as a superposition of eigenmodes of Eq. (9). The downward irradiance $E_d(z) = E_+(z)$ and the upward irradiance $E_u(z) = E_-(z)$ are obtained from an integration of the radiance over μ with Eqs. (6) and (7):

$$E_\pm(z) = \sum_{j=1}^{J} [C(\nu_j)\tilde{g}_1(\pm\nu_j)\exp(-cz/\nu_j) + C(-\nu_j)\tilde{g}_1(\mp\nu_j)\exp(cz/\nu_j)], \quad \text{(A1)}$$

where

$$\tilde{g}_1(\nu_1) = \int_0^1 \phi(\nu_1, \mu)\mu d\mu,$$

$$\tilde{g}_1(-\nu_1) = \int_{-1}^0 \phi(\nu_1, \mu)|\mu|d\mu = \int_0^1 \phi(-\nu_1, \mu)\mu d\mu, \quad \text{(A2)}$$

and the expansion coefficients $C(\pm\nu_j)$ depend on the IOP's and the surface illumination and bottom albedo boundary conditions. Beyond a couple of optical depths from either of the boundaries, the eigenvalues $\pm\nu_1$ make the dominant contributions so Eq. (A1) can be approximated by

$$E_\pm(z) \approx C(\nu_1)\tilde{g}_1(\pm\nu_1)\exp(-cz/\nu_1) + C(-\nu_1)\tilde{g}_1(\mp\nu_1)\exp(cz/\nu_1), \quad \text{(A3)}$$

and for deep waters where there are no bottom effects, $C(-\nu_1) \to 0$ and

$$R_\infty = \tilde{g}_1(-\nu_1)/\tilde{g}_1(\nu_1), \quad \text{(A4)}$$

which is Eq. (13). In a similar manner, use of Eq. (A3) with $C(-\nu_1) = 0$ and Eq. (8) yields K_∞ of Eq. (14).

Appendix B: Relationship between the Sensitivity Coefficients of the Forward and Inverse Problems

The sensitivity coefficients for the inverse problem (the computation of ω_0 and ν_1 from R_∞ and g) can be computed more easily when they are expressed in terms of partial derivatives of the forward problem (the computation of R_∞ and ν_1 from ω_0 and g). Let the superscript f denote forward-problem variables, which depend on ω_0 and g, and unmarked variables denote inverse-problem variables. If we make a transformation of variables and use the Jacobian of the transformation, it follows that

$$\frac{\partial\omega_0}{\partial R_\infty} = \frac{1}{\partial R_\infty^f/\partial\omega_0}, \quad \text{(B1)}$$

$$\frac{\partial\omega_0}{\partial g} = -\frac{1}{\partial R_\infty^f/\partial\omega_0}\frac{\partial R_\infty^f}{\partial g}, \quad \text{(B2)}$$

where R_∞^f is computed directly from Eq. (13). These results are consistent with those of Fig. 2. Furthermore, from the chain rule and the previous two equations,

$$\frac{\partial\nu_1}{\partial R_\infty} = \frac{\partial\nu_1^f}{\partial\omega_0}\frac{\partial\omega_0}{\partial R_\infty} = \frac{\partial\nu_1^f}{\partial\omega_0}\frac{1}{\partial R_\infty^f/\partial\omega_0}, \quad \text{(B3)}$$

$$\frac{\partial\nu_1}{\partial g} = \frac{\partial\nu_1^f}{\partial g} + \frac{\partial\nu_1^f}{\partial\omega_0}\frac{\partial\omega_0}{\partial g} = \frac{\partial\nu_1^f}{\partial g} - \frac{\partial\nu_1^f}{\partial\omega_0}\frac{1}{\partial R_\infty^f/\partial\omega_0}\frac{\partial R_\infty^f}{\partial g}. \quad \text{(B4)}$$

Appendix C: Estimation of the Asymptotic Irradiance Ratio Near the Bottom

1. Derivation of the DMRM

From Eqs. (A3) and (A4),

$$E_+(z) \pm E_-(z) \approx \tilde{g}_1(\nu_1)(1 \pm R_\infty)[C(\nu_1)\exp(-cz/\nu_1) \pm C(-\nu_1)\exp(cz/\nu_1)]. \quad \text{(C1)}$$

After squaring the last equation we can see that

$$[E_+(z) \pm E_-(z)]^2 \approx \tilde{g}_1{}^2(\nu_1)(1 \pm R_\infty)^2[C^2(\nu_1) \times \exp(-2cz/\nu_1) + C^2(-\nu_1) \times \exp(2cz/\nu_1) \pm 2C(\nu_1)C(-\nu_1)]. \quad \text{(C2)}$$

Equation (42) follows after we evaluate this equation at two depths z_1 and z_2 and take the difference of the results.

2. Derivation of the SMRM

From Eqs. (A3) and (A4),

$$R(z) = \frac{E_-(z)}{E_+(z)} = \frac{R_\infty + C(-\nu_1)\exp(2cz\nu_1)/C(\nu_1)}{1 + C(-\nu_1)R_\infty \exp(2cz/\nu_1)/C(\nu_1)}, \quad \text{(C3)}$$

so it follows that

$$R(z) - R_\infty = \frac{C(-\nu_1)(1 - R_\infty)\exp(2cz/\nu_1)/C(\nu_1)}{1 + R_\infty C(-\nu_1)\exp(2cz/\nu_1)/C(\nu_1)}. \quad \text{(C4)}$$

For z in Eq. (C4) just below the surface,

$$R(0^+) - R_\infty = \frac{C(-\nu_1)(1 - R_\infty)/C(\nu_1)}{1 + R_\infty C(-\nu_1)/C(\nu_1)}, \quad \text{(C5)}$$

whereas for z in Eq. (C4) at the bottom, $z = z_b$, the reflectance equals the bottom albedo R_b, and

$$R_b - R_\infty = \frac{C(-\nu_1)(1 - R_\infty)\exp(2cz_b/\nu_1)/C(\nu_1)}{1 + R_\infty C(-\nu_1)\exp(2cz_b/\nu_1)/C(\nu_1)}. \quad \text{(C6)}$$

From Eqs. (C5) and (C6),

$$(R_b - R_\infty)\exp(-2cz_b/\nu_1) = \frac{[R(0^+) - R_\infty][1 + C(-\nu_1)R_\infty/C(\nu_1)]}{1 + R_\infty C(-\nu_1)\exp(2cz_b/\nu_1)/C(\nu_1)}. \quad \text{(C7)}$$

If $R_\infty C(-\nu_1)/C(\nu_1) \ll 1$, then

$$(R_b - R_\infty)\exp(-2cz_b/\nu_1) \approx R(0^+) - R_\infty. \quad \text{(C8)}$$

It follows that if the bottom albedo is known and $K_\infty = c/\nu_1$ is estimated from $E_d(z)$, then R_∞ can be estimated from $R(0^+)$:

$$R_\infty = [R(0^+) - R_b \exp(-2K_\infty z_b)]/[1 - \exp(-2K_\infty z_b)]. \quad \text{(C9)}$$

This equation has been used by others, e.g., Ref. 27. Equation (43) is a generalization away from $z = 0^+$ and uses either the local $K_d(z)$ or the best estimate of K_∞.

This research was supported by the U.S. Office of Naval Research and by the San Diego Supercomputer Center. We thank Howard Gordon, Vladimir Haltrin, Emmanuel Boss, Lydia Sundman, and the reviewers for helpful suggestions and Knut Stamnes for providing us with the computer code DISORTB.

References

1. R. W. Preisendorfer, *Hydrologic Optics*, V.1. NTIS PB 259793/8ST (National Technical Information Service, Springfield, Va., 1976).
2. D. A. Kiefer and B. G. Mitchell, "A simple, steady-state description of phytoplankton growth based on absorption cross section and quantum efficiency," Limnol. Oceanogr. **28,** 770–776 (1983).
3. M. Kishino, "Interrelationship between light and phytoplankton in the sea," in *Ocean Optics*, R. W. Spinrad, K. L. Carder, and M. J. Perry, eds. (Oxford U. Press, New York, 1994).
4. A. A. Gershun, "The light field," J. Math. Phys. (Cambridge, Mass.) **18,** 51–151 (1939).
5. K. L. Carder, D. J. Collins, M. J. Perry, H. L. Clark, J. M. Mesias, J. S. Cleveland, and J. Greenier, "The interaction of light with phytoplankton in the marine environment," in *Ocean Optics VIII*, M. A. Blizard, ed., Proc. SPIE **637,** 42–55 (1986).
6. L. Prieur and S. Sathyendranath, "An optical classification of coastal and oceanic waters based on the specific spectral absorption curves of phytoplankton pigments, dissolved organic matter, and other particulate materials," Limnol. Oceanogr. **26,** 671–689 (1981).
7. J. R. V. Zaneveld, "A reflecting tube absorption meter," in *Ocean Optics X*, R. W. Spinrad, ed., Proc. SPIE **1302,** 124–136 (1990).
8. H. R. Gordon, "Modeling and simulating radiative transfer in the ocean," in *Ocean Optics*, R. W. Spinrad, K. L. Carder, and M. J. Perry, eds. (Oxford U. Press, New York, 1994).
9. H. R. Gordon and G. C. Boynton, "A radiance–irradiance inversion algorithm for estimating the absorption and backscattering coefficients of natural waters: homogeneous waters," Appl. Opt. **36,** 2636–2641 (1997).
10. Z. Tao, N. J. McCormick, and R. Sanchez, "Ocean source and optical property estimation using explicit and implicit algorithms," Appl. Opt. **33,** 3265–3275 (1994).
11. S. Chandrasekhar, *Radiative Transfer* (Oxford U. Press, New York, 1950).
12. M. Benassi, R. D. M. Garcia, A. H. J. Karp, and C. E. Siewert, "A high-order spherical harmonics solution to the standard problem in radiative transfer," Astrophys. J. **280,** 853–864 (1984).
13. N. J. McCormick, "Asymptotic optical attenuation," Limnol. Oceanogr. **37,** 1570–1578 (1992).
14. C. E. Siewert, "The F_N method for solving radiative-transfer problems in plane geometry," Astrophys. Space Sci. **58,** 131–137 (1978).
15. L. C. Henyey and J. L. Greenstein, "Diffuse radiation in the galaxy," Astrophys. J. **93,** 70–83 (1941).
16. K. Stamnes, "The Chandrasekhar method and its applications to atmospheric radiative transfer," Trans. Am. Nucl. Soc. **71,** 213–214 (1994).
17. Z. Jin and K. Stamnes, "Radiative transfer in nonuniformly refracting layered media such as the atmosphere/ocean system," Appl. Opt. **33,** 431–442 (1994).
18. N. J. McCormick, "Analytical transport theory applications in optical oceanography," Ann. Nucl. Energy **23,** 381–395 (1996).
19. J. R. V. Zaneveld, "An asymptotic closure theory for irradiance in the sea and its inversion to obtain the inherent optical properties," Limnol. Oceanogr. **34,** 1442–1452 (1989).
20. N. J. McCormick, "Mathematical models for the mean cosine of irradiance and the diffuse attenuation coefficient," Limnol. Oceanogr. **40,** 1013–1018 (1995).
21. H. R. Gordon, O. B. Brown, and M. M. Jacobs, "Computed relationships between the inherent and apparent optical properties of a flat homogeneous ocean," Appl. Opt. **14,** 417–427 (1975).
22. W. H. Press, B. P. Flannery, S. A. Teukolsky, and W. T. Vet-

terling, *Numerical Recipes* (Cambridge U. Press, New York, 1989), pp. 274–286.
23. T. J. Petzold, "Volume scattering functions for selected ocean waters," SIO Ref. 72-78 (Scripps Institution of Oceanography, Visibility Laboratory, San Diego, Calif., 1972).
24. P. W. Francisco and N. J. McCormick, "Chlorophyll concentration effects on asymptotic optical attenuation," Limnol. Oceanogr. **39,** 1195–1205 (1994).
25. G. W. Kattawar, "A three-parameter analytic phase function for multiple scattering calculations," J. Quant. Spectrosc. Radiat. Transfer **15,** 839–849 (1975).
26. V. I. Haltrin, "Algorithm for computing apparent optical properties of shallow waters under arbitrary surface illumination," in *Proceedings of the International Airborne Remote Sensing Conference and Exhibition* (Environmental Research Institute of Michigan, Ann Arbor, Mich., 1997), pp. 463–470.
27. N. T. O'Neill, A. R. Kalinauskas, J. D. Dunlop, A. B. Hollinger, H. Edel, M. Casey, and J. Gibson, "Bathymetric analysis of geometrically corrected imagery data collected using a two dimensional imager," in *Ocean Optics VIII*, M. A. Blizard, ed., Proc. SPIE **637,** 191–202 (1986).